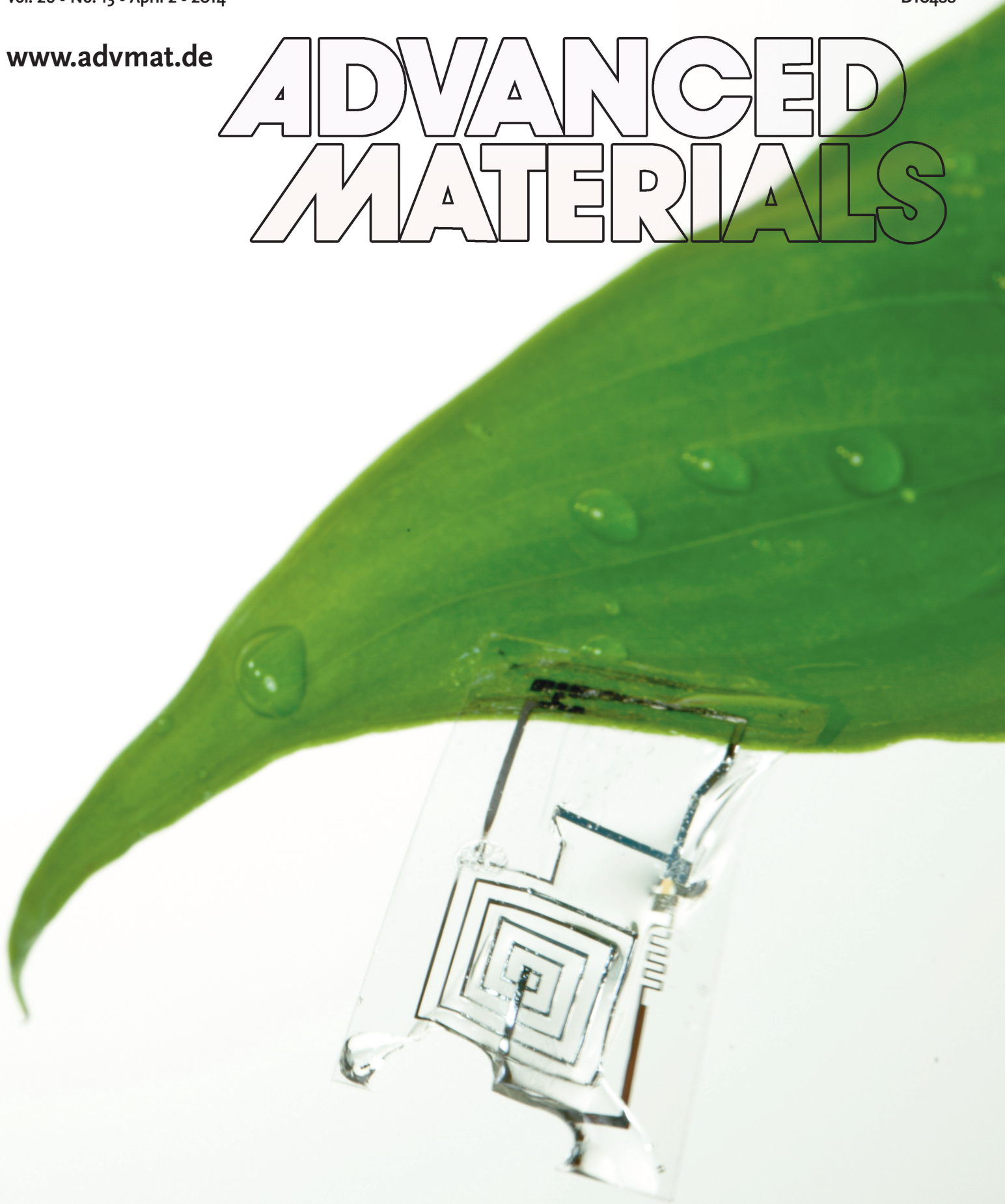


[www.advmat.de](http://www.advmat.de)

# ADVANCED MATERIALS



# 25th Anniversary Article: Materials for High-Performance Biodegradable Semiconductor Devices

Suk-Won Hwang, Gayoung Park, Huanyu Cheng, Jun-Kyul Song, Seung-Kyun Kang, Lan Yin, Jae-Hwan Kim, Fiorenzo G. Omenetto, Yonggang Huang, Kyung-Mi Lee,\* and John A. Rogers\*

We review recent progress in a class of silicon-based electronics that is capable of complete, controlled dissolution when immersed in water or bio-fluids. This type of technology, referred to in a broader sense as transient electronics, has potential applications in resorbable biomedical devices, eco-friendly electronics, environmental sensors, secure hardware systems and others. New results reported here include studies of the kinetics of hydrolysis of nanomembranes of single crystalline silicon in bio-fluids and aqueous solutions at various pH levels and temperatures. Evaluations of toxicity using live animal models and test coupons of transient electronic materials provide some evidence of their biocompatibility, thereby suggesting potential for use in bioresorbable electronic implants.

## 1. Introduction

Electronic systems built entirely with biocompatible and biodegradable materials are of growing interest for future classes of implantable devices. Such systems, sometimes viewed as part of a broader class of a technology referred to as transient electronics, can be configured to provide diagnostic and/or therapeutic function during, for example, a wound healing process. Following this function, the devices disappear completely, thereby eliminating unnecessary load on the body. Early work examined partially resorbable electronics built

using thin, miniaturized inorganic components on resorbable silk supports,<sup>[1,2]</sup> and, in separate studies, using various biological or synthetic organic active and passive materials.<sup>[3,4]</sup> An important recent advance<sup>[5]</sup> in this field followed the realization that semiconductor grade, monocrystalline silicon can undergo hydrolysis at physiological conditions, with rates that can be relevant for envisioned applications in biomedicine. Resorbable nanoporous silicon matrices designed for non-electronic drug delivery vehicles provide some precedent<sup>[6,7]</sup> for the associated chemistry. Combining nanomembranes of silicon (Si NMs) with

other thin film inorganic materials such as magnesium and magnesium oxide for conductors and insulators, respectively, forms a route to integrated circuits, sensors, communication devices and power supply systems.<sup>[5,8,9]</sup> Reported examples include a complimentary metal-oxide semiconductor (CMOS) technology, sensors for strain and temperature, solar cells, digital imaging arrays, wireless power harvesting circuits and others.<sup>[5,8–10]</sup> This article reviews recent progress in transient electronics, and presents new studies of the kinetics of silicon hydrolysis in various solutions. Results from *in vivo* investigations provide information on biocompatibility.

Dr. S.-W. Hwang, J.-K. Song, Dr. S.-K. Kang,  
Dr. L. Yin, J.-H. Kim  
Department of Materials Science and Engineering  
Frederick Seitz Materials Research Laboratory  
University of Illinois at Urbana-Champaign  
Urbana, IL 61801, USA

Prof. J. A. Rogers  
Department of Materials Science and Engineering  
Chemistry, Mechanical Science and Engineering  
Electrical and Computer Engineering  
Beckman Institute for Advanced Science and Technology  
and Frederick Seitz Materials Research Laboratory  
University of Illinois at Urbana-Champaign  
Urbana, IL 61801, USA  
E-mail: jrogers@illinois.edu

G. Park, Prof. K.-M. Lee  
Global Research Laboratory  
Department of Biochemistry and Molecular Biology  
Korea University College of Medicine  
Seoul, 136-713, Republic of Korea  
E-mail: kyunglee@korea.ac.kr

H. Cheng, Prof. Y. Huang  
Department of Mechanical Engineering  
Civil and Environmental Engineering  
Center for Engineering and Health  
and Skin Disease Research Center  
Northwestern University  
Evanston, IL 60208, USA  
Prof. F. G. Omenetto  
Department of Biomedical Engineering  
Tufts University  
Medford, MA 02155, USA



DOI: 10.1002/adma.201304821

## 2. Results and Discussion

**Figure 1** shows examples of transient electronic devices<sup>[8–10]</sup> that use biocompatible inorganic electronic materials, including silicon (Si) and zinc oxide (ZnO) as semiconductors, magnesium (Mg) as conductors, and magnesium oxide (MgO) and silicon dioxide (SiO<sub>2</sub>) as dielectrics. Other recently studied metals include Zn, W, Mo and Fe.<sup>[11]</sup> Films of silk fibroin are attractive as substrates and encapsulation layers.<sup>[5]</sup> Figure 1a presents, as an example of an integrated system, a silicon-based radio frequency (RF) power scavenger that incorporates a collection of RF diodes, an inductor and capacitors, with electrode pads for connections to an antenna and a light emitting diode (LED, to visually demonstrate function). The entire circuit dissolves upon immersion in water, starting with disappearance of the silk substrate, then spontaneous fracture and disintegration of the other materials into small fragments, each of which undergoes reaction to yield soluble hydroxides (Figure 1b).<sup>[8]</sup> This last process is illustrated most clearly through studies on non-transient substrates, as shown for the case of a ZnO thin film transistor (TFT) in the optical microscopy images of Figure 1c.<sup>[10]</sup> Here, all constituent materials completely dissolve in ~15 hours; the main reaction products are Zn(OH)<sub>2</sub> for ZnO, and Mg(OH)<sub>2</sub> for Mg and MgO, respectively. The case of an inverter based on Si metal oxide semiconductor field effect transistors (MOSFETs), tethered in a suspended geometry to a silicon wafer support, appears schematically in Figure 1d.<sup>[9]</sup> The sequence of optical microscopy images in Figure 1e illustrates dissolution of this type of device. The Mg source, drain and gate contacts react to form Mg(OH)<sub>2</sub> during the first ~10 hours. Removal of buried Mg leads to fracture in overlying layers of SiO<sub>2</sub>, and accelerated dissolution. Next, the SiO<sub>2</sub> (gate dielectric; low density, deposited by plasma-enhanced chemical vapor deposition, PECVD) and the Si NM (active layer) dissolve as Si(OH)<sub>4</sub>,<sup>[12–14]</sup> over a period of ~4 weeks. The SiO<sub>2</sub> (high density, grown thermally) at the base dissolves very slowly under these conditions (phosphate buffered saline (PBS) solution, at pH 7.4 and 37 °C).

Figure 1f presents measured changes in the electrical characteristics of an inverter encapsulated with MgO (~800 nm), as a function of time following immersion in deionized (DI) water at room temperature. The properties remain unchanged for ~7 hours, and then rapidly degrade (i.e. transience in function) in the following ~50 min. Dissolution of Mg is responsible for degradation in function. In this way, the devices offer i) stable performance for a time set by dissolution of the transient encapsulation layer, followed by ii) rapid functional degradation at a rate set by the transient electrodes (e.g. Mg). This type of controlled, two-stage behavior in transience is important for many envisioned applications.

Various active and passive electronic components and sensors can be built using these transient materials. **Figure 2** presents images and electrical characteristics of examples ranging from strain sensors,<sup>[5]</sup> to temperature gauges,<sup>[5]</sup> solar cells,<sup>[5]</sup> ring oscillators<sup>[8]</sup> and mechanical energy harvesters.<sup>[10]</sup> Highly doped Si NMs with Mg interconnects and silk substrates can be used to form mechanically flexible strain gauges, as in Figure 2a; fractional changes in resistance due to bending indicate gauge factors of ~40. Arrays of Si diodes can serve as temperature



**Suk-Won Hwang** received B.S. and M.S. degrees in the Department of Material Science and Engineering from the Hanyang University, Korea. After graduation, he worked for Samsung Electronics Co., LTD (2005 ~ 2007), and developed the world's first 16 G NAND Flash Memory as a member of team. He obtained a Ph.D degree under the guidance of Professor John A. Rogers, in the Departments of Materials Science and

Engineering at the University of Illinois at Urbana-Champaign with support from the Fulbright Fellowship. He currently works under Professor John A. Rogers as a postdoctoral research fellow.



**Kyung-Mi Lee** is professor in the Department of Biochemistry and Molecular Biology at the Korea University College of Medicine and project leader of a Korean Global Research Laboratory focused on world-wide collaborative studies in immunobiology field. She obtained B.S. and M.S. degrees from the College of Pharmacy at Seoul National University in 1989 and Ph. D. in the department of Pharmacology and Physiology at the University of Chicago in 1995.

She completed postdoctoral training at Harvard Medical School, was appointed as an instructor and research associate professor at the University of Chicago. Since joining the faculty at Korea University in 2003, her research focus in the area of tumor immunology and transplantation has led to the development of novel translational approaches for the treatment of patients with cancer and autoimmune disease. Her laboratory has been involved in cross-disciplinary efforts in biomedical engineering and the development of unique biomaterial platform for immune cell detection, selection, and expansion as a means of enhancing the human immune response both in vitro and in vivo.



**John A. Rogers** obtained B.A. and B.S. degrees in chemistry and in physics from the University of Texas, Austin, in 1989. From MIT, he received S.M. degrees in physics and in chemistry in 1992 and a Ph.D. in physical chemistry in 1995. From 1995 to 1997, Rogers was a Junior Fellow in the Harvard University Society of Fellows. He joined Bell Laboratories as a Member of Technical Staff in the Condensed Matter Physics Research Department in 1997, and served as Director of

this department from 2000-2002. He currently holds the Swarlund Chair at the University of Illinois at Urbana-Champaign, with appointments in the departments of Materials Science and Engineering, Electrical and Computer Engineering, Mechanical Science and Engineering and Chemistry. Rogers' research includes fundamental and applied aspects of nano and molecular scale fabrication, materials and patterning techniques for unusual format electronics and photonic systems.

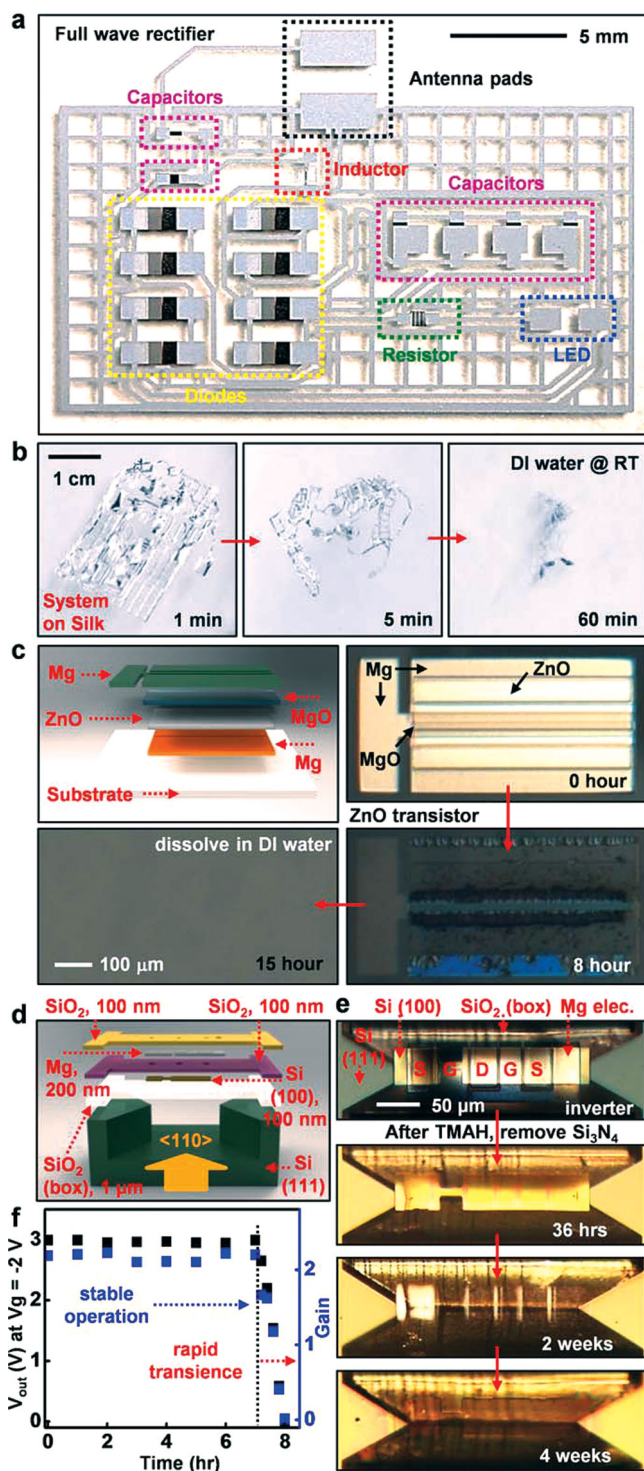


**Figure 1.** Representative transient electronic devices, their dissolution behaviors and electrical properties. (a) Image of a transient RF power harvesting system (left), built using silicon nanomembranes (Si NMs, semiconductors), magnesium (Mg, electrodes and interconnects), silicon dioxide (SiO<sub>2</sub>, interlayer dielectrics), and films of silk fibroin (substrate and encapsulant). The circuit includes RF diodes (rectifiers), capacitors, an inductor, a resistor and electrode pads for connection to an antenna and a light emitting diode (LED, to visually indicate function). Reproduced with permission.<sup>[8]</sup> 2013, Wiley. (b) A time sequence of images collected

sensors (Figure 2b), solar cells (Figure 2c) and photodetectors. Sensitivity for temperature mapping is  $-2.23 \text{ mV}/^\circ\text{C}$  (change in voltage for a given current output), and the efficiency for solar power conversion is  $\sim 3\%$ . RF operation provides additional options in power supply (Figure 1a), as well as means for radio communication. Figure 2d shows three-stage CMOS ring oscillators built using MOSFETs based on Si NMs. Oscillation frequencies vary from  $\sim 2.6 \text{ MHz}$  to  $4.1 \text{ MHz}$ , depending on applied bias ( $V_{\text{dd}}$ ), 10V (black), 15 V (red) and 20 V (blue). Improvements are possible through reductions in critical feature sizes of the devices. ZnO represents an alternative semiconductor, of interest due to its direct bandgap and piezoelectric properties. Figure 3 e shows an array of flexible mechanical energy harvesters that use Mg electrodes as top and bottom contacts to thin films of ZnO. Bending induces tensile and compressive strains that enable extraction of electrical power from the ZnO. For the example shown here, bending produces peak output voltages and currents of  $\sim 1.14 \text{ V}$  and  $\sim 0.55 \text{ nA}$ , respectively.

Knowledge of the chemical kinetics for reactions in transient electronic materials is essential to the development of this technology. Hydrolysis of Si NMs is particularly important. Literature studies involving basic aqueous solutions suggest that silicon can either form neutral ortho-silicic acid Si(OH)<sub>4</sub> through an initial oxidation step to SiO<sub>2</sub> or through a direct equilibrium  $\text{Si} + 4\text{H}_2\text{O} \leftrightarrow \text{Si(OH)}_4 + 2\text{H}_2$ .<sup>[12,13,15]</sup> In both cases, the silicic acid leaves the silicon surface by diffusion into the surrounding solution. The details depend not only on the crystalline form and morphology of the silicon, its doping level and other parameters, but also on the temperature and composition of the solution.<sup>[12,16–22]</sup> **Figure 3** summarizes the kinetics observed for Si NMs in bio-fluids and aqueous solutions at different pH and temperature. Experiments here involve buffer solutions (pH 6 to 14, Sigma-Aldrich, USA) and arrays of Si NMs patterned into squares ( $3 \mu\text{m} \times 3 \mu\text{m} \times 70 \text{ nm}$ ) on SiO<sub>2</sub>/Si substrates ( $1 \text{ cm} \times 1.5 \text{ cm}$ ), created using silicon on insulator (SOI) wafers. Inserting the samples into aqueous buffer solutions (50 mL, in a petri dish with diameter of 7 cm), removing them after a certain time, measuring the Si NM thickness by atomic force microscopy (AFM), and then re-inserting the samples back into a fresh buffer solution, reveals the thickness as a function of immersion time. The trends with temperature

during dissolution in deionized (DI) water. Reproduced with permission.<sup>[8]</sup> 2013, Wiley. (c) Exploded view schematic illustration of a water soluble thin film transistor that uses zinc oxide (ZnO, semiconductor), Mg (source, drain, gate) and MgO (gate dielectric) (top left). Optical microscopy images of a device before (0 hour), and after 8 and 15 hours of immersion in DI water. Complete dissolution occurs in  $\sim 15$  hours. Reproduced with permission.<sup>[10]</sup> 2013, Wiley. (d) Exploded view schematic illustration of a transient inverter device, tethered in a suspended configuration to an underlying silicon wafer. The release in this case used anisotropic wet chemical etching of the substrate, which has (111) orientation. Reproduced with permission.<sup>[9]</sup> 2013, Wiley. (e) Time sequence of optical microscopy images showing dissolution of a transient inverter in phosphate buffer saline (PBS, 1 M, pH 7.4) solution at physiological temperature ( $37^\circ\text{C}$ ). Reproduced with permission.<sup>[9]</sup> 2013, Wiley. (f) Measured changes in the electrical properties of a transient inverter encapsulated with MgO ( $\sim 800 \text{ nm}$ ) as a function of time of immersion in water. The output voltages (at  $V_{\text{g}} = -2 \text{ V}$ ) and gain (right) illustrate stable operation for  $\sim 7$  hours, followed by rapid degradation in  $\sim 50 \text{ min}$ . Reproduced with permission.<sup>[9]</sup> 2013, Wiley.

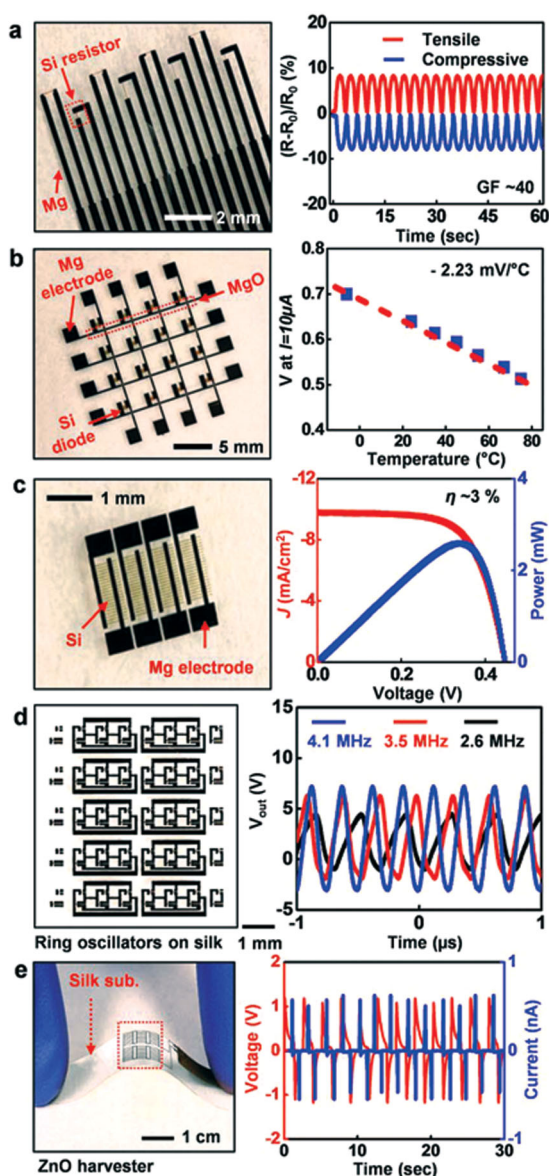


**Figure 2.** Images and electrical characteristics of transient electronic components, sensors and simple circuits. (a) Image of an array of strain gauges that use Si NMs and Mg electrodes (left), and fractional change in resistance during bending to induce tensile (red) and compressive (blue) strains (right). Reproduced with permission.<sup>[5]</sup> 2013, AAAS. (b) Optical image of a  $4 \times 4$  array of temperature sensors based on Si NM diodes. Mg and MgO serve electrodes as interconnects and interlayer dielectrics, respectively (left). Changes in voltage (at  $I = 10 \mu\text{A}$ ) at different temperatures illustrate a sensitivity of  $\sim -2.23 \text{ mV}/^\circ\text{C}$ . Reproduced with permission.<sup>[5]</sup> 2013, AAAS. (c) Image of transient solar cells built using narrow strips of Si ( $\sim 3 \mu\text{m}$  thick) with Mg contacts and interconnects (left). Current density (red) and power (blue) measured as a function of voltage while illuminated by a solar simulator. Reproduced with permission.<sup>[5]</sup> 2013, AAAS. (d) Image of a set of Si NM based CMOS three stage ring oscillators, with Mg contacts and interconnects and MgO gate dielectrics (left). Time responses of a ring oscillator at different operating frequencies between 2.5 and 4 MHz. Reproduced with permission.<sup>[8]</sup> 2013, Wiley. (e) Image of a flexible array of transient ZnO energy harvesters/strain gauges (left). Measured output voltage (red) and current (blue) as a function of time during cyclic loading (right). Reproduced with permission.<sup>[10]</sup> 2013, Wiley.

and pH can be captured using a simple, linear model of reactive diffusion, with a constant dissolution rate at the solution/Si NM interface.<sup>[12]</sup> This model assumes no diffusion of molecules from the solution into the silicon, and accounts only for surface reactions, thereby leading to linear dissolution behavior. In particular, the thickness ( $h$ ) at time ( $t$ ) can be related to the initial thickness ( $h_0$ ) and the dissolution rate ( $R$ ) measured as the change in thicknesses of Si NM per unit time as  $h = h_0 - Rt$ . The straight lines that appear in the plots of Figure 3a, b and d correspond to the results of such a model, fit to the data. A previously reported scaling relationship<sup>[12]</sup> relates the dissolution rate ( $R$ ) of silicon, to the temperature  $T$  and molar concentrations of water [ $\text{H}_2\text{O}$ ] and hydroxide ions [ $\text{OH}^-$ ] by

$$R = k_0 [\text{H}_2\text{O}]^4 [\text{OH}^-]^{\frac{1}{4}} e^{-\frac{E_A}{k_B T}}, \quad (1)$$

where  $k_B$  is the Boltzmann constant and  $E_A$  is the activation energy. This equation captures experimental trends for dissolution in high pH solutions of KOH, when  $k_0 = 2480 \mu\text{m}/\text{h}$  ( $\text{mol}/\text{liter}$ )<sup>-4.25</sup>,  $E_A = 0.595 \text{ eV}$ .<sup>[12]</sup> For the solutions examined in the present work, where the pH falls into significantly lower range, the water concentration does not vary significantly. Here, the functional dependencies represented Equation (1) can account for observed dissolution rates, measured as the change in thicknesses of Si NM per unit time, for pH and temperature ranges from 6 to 14 and from room to physiological temperature, respectively (Figure 3c), but with a different power law exponent (0.55) for [ $\text{OH}^-$ ], and with  $k_0 = 7045 \text{ nm}/\text{day}$  ( $\text{mol}/\text{liter}$ )<sup>-4.55</sup> and  $E_A = 0.404 \text{ eV}$ . The pH levels, and concentration and type of ions in the solution can both have significant effects on the process, in terms of rates as well as other qualitative aspects. For example, solutions of KOH dissolve the silicon in an anisotropic fashion; dissolution in buffer solutions, for the cases examined here, occurs isotropically. Figure 3d shows that the rate increases with molar concentration of phosphate buffer solution (at fixed pH and temperature), in a manner that is qualitatively consistent with previous studies of the effects of NaCl and KCl on the dissolution of  $\text{SiO}_2$ , near neutral pH.<sup>[23,24]</sup> (In this context, we note that the name/property of commercial phosphate buffer solutions (1 M, pH 7.4, Sigma-Aldrich, USA) recently changed, leading to an increase of dissolution rate of Si NMs by up to 10 ~ 20 times. Here, we refer to this new solution as 'new 1M'.) Given the complexity of the underlying chemical processes, it is important to examine directly the dissolution behaviors in relevant biofluids and water in natural environmental conditions to assess properties relevant to envisioned applications in biomedicine and 'green' electronics, respectively. The case of bovine serum (pH  $\sim 7.4$ , Sigma-Aldrich, USA) appears in Figure 3e, where the dissolution rates are  $\sim 1.6 \text{ nm}/\text{hour}$  and  $\sim 4.2 \text{ nm}/\text{hour}$  at room temperature and body temperature, respectively. These values are somewhat higher than those observed at similar pH in buffer solution due possibly to the influence of various chemical components present in the serum. Dissolution in sea water, which has a pH similar to bovine serum, occurs at somewhat slower rates (Figure 3f).

The results of Figure 3e demonstrate transience in a context relevant for use in the body. Initial *in vivo* evaluations involved implantation of simple transient electronic devices in the sub-dermal region of BALB/c mice in accordance with

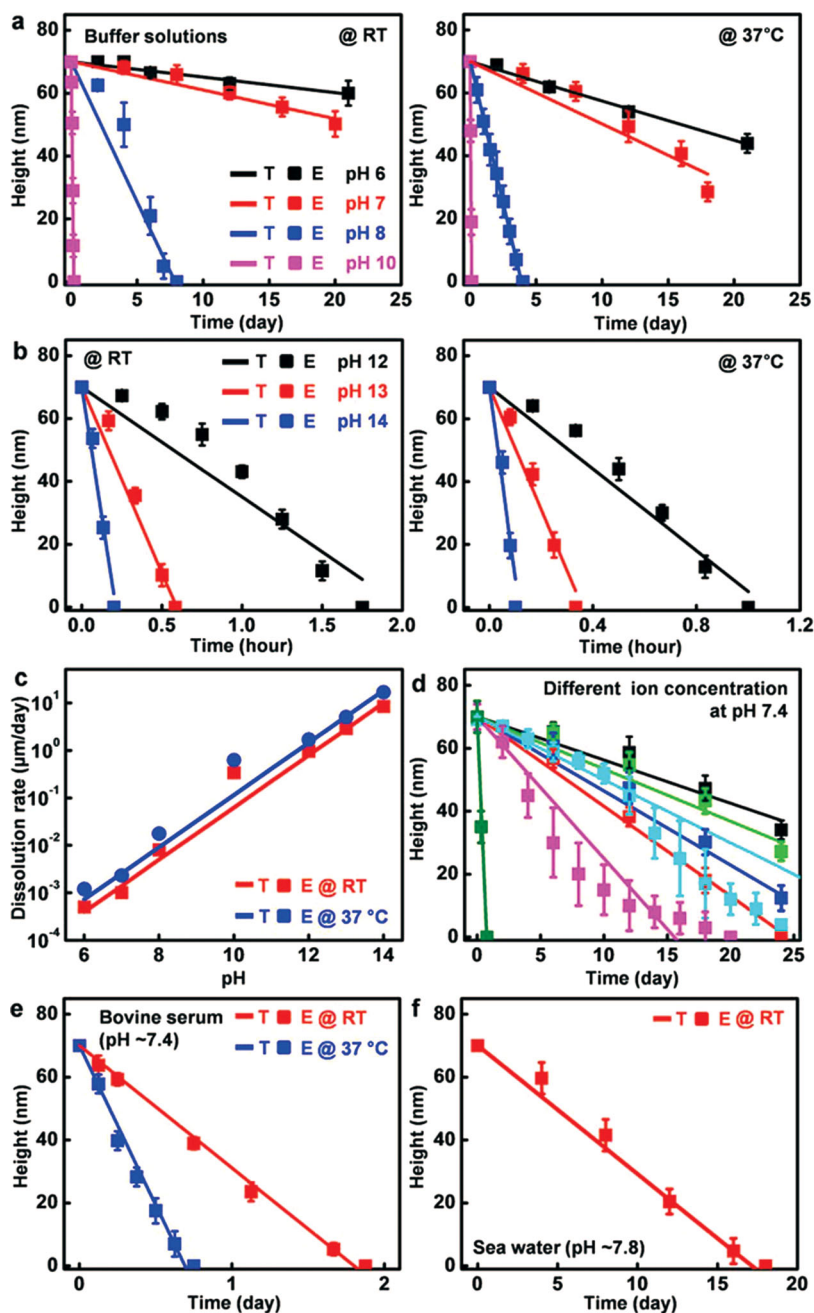


**Figure 3.** Hydrolysis of silicon nanomembranes (Si NMs) in bio-fluids and in aqueous solutions at different pH levels and temperatures. (a) Theoretical (T, lines) and experimental (E, symbols) dissolution of Si NMs ( $3 \mu\text{m} \times 3 \mu\text{m} \times 70 \text{nm}$ ) in buffer solutions at different pH (pH 6, black; pH 7, red; pH 8, blue; pH 10, purple), at room temperature (left) and physiological temperature (right,  $37^\circ\text{C}$ ). (b) Calculated (T, lines) and measured (E, symbols) dissolution of Si NMs ( $3 \mu\text{m} \times 3 \mu\text{m} \times 70 \text{nm}$ ) during immersion in buffer solutions with higher pH (pH 12, black; pH 13, red; pH 14, blue), at room temperature (left) and physiological temperature (right,  $37^\circ\text{C}$ ). (c) Theoretical (T, lines) and experimental (E, symbols) dissolution rates of Si NMs as a function of pH in buffer solutions, at room temperature (red) and  $37^\circ\text{C}$  (blue). (d) Theoretical (T, lines) and experimental (E, symbols) results of the dependence of ionic concentration of phosphate buffer solutions (pH 7.4) on Si dissolution rate. (black, 0.05 M at RT; blue, 0.05 M at  $37^\circ\text{C}$ ; green, 0.1 M at RT; red, 0.1 M at  $37^\circ\text{C}$ ; cyan, 1 M at RT; purple, 1 M at  $37^\circ\text{C}$ ; olive, New 1 M at  $37^\circ\text{C}$ ) (e) Calculated (T, lines) and measured values (E, symbols) of Si dissolution rate in bovine serum (pH  $\sim 7.4$ ) at room temperature and physiological temperature ( $37^\circ\text{C}$ ). (f) Theoretical model (lines) and experimental data (dots) of silicon dissolution rate in sea water (pH  $\sim 7.8$ ) at room temperature.

Institutional Animal Care and Use Committee (IACUC)-approved protocols, as shown in Figure 4.<sup>[5]</sup> Examination after 3 weeks revealed that the implants disappeared without any visible remnants of the constituent materials (Figure 4b, left). The histological section shows the sub-dermal layer (A), the silk film (B) and the muscle layer (C), all without any significant inflammatory response (Figure 4b, right). Additional work reported here involves long term immunologic and tissue biocompatibility, in a protocol in which 2 cm long sagittal skin incisions on the upper back of the mouse created subcutaneous pockets on both the left and right sides. A piece of high-density polyethylene (HDPE), as a control, is implanted on the left side of the mouse; a test structure built with transient electronic materials is implanted on the right side. Both wounds are closed with metallic clips. Mice are then returned to a specific pathogen free (SPF) facility and monitored for 5 weeks. The test structures use films of silk fibroin ( $5 \text{mm} \times 10 \text{mm} \times 25 \mu\text{m}$ ), sterilized by ethylene oxide, as substrates for four different types of samples with various patterned shapes: bare silk, Si NMs ( $400 \mu\text{m} \times 400 \mu\text{m} \times 70 \text{nm}$ ) on silk, Mg ( $400 \mu\text{m} \times 400 \mu\text{m} \times 300 \text{nm}$ ) on silk, and MgO ( $400 \mu\text{m} \times 400 \mu\text{m} \times 300 \text{nm}$ ) on silk. In all cases, the implanted mice (a total of 8 with each type of sample) behave normally with increases in their body weight in parallel to that of the sham-operated controls. No serious adverse events or complications occur during the evaluation period. Following 5 weeks of implantation, immunoprofiling of lymphocytes from the peripheral blood and draining lymph nodes reveal no significant differences in the percentages of CD4+ and CD8+ T cells for implanted animals and sham-operated controls. For mice implanted with Mg on silk, the percentages of B cells in the blood are slightly higher than sham-operated mice; no differences are observed for the other types of implants. The percentages of NK cells in the blood are slightly lower in mice implanted with Mg on silk and MgO on silk compared to sham-operated mice (Figure 5a). Although the underlying causes of these changes are unknown, reductions in NK cell percentages could correlate to increases in B cells. The immune profile in the axillary and branchial draining lymph nodes (DLNs) provide insights into whether these changes persist in lymph nodes that lie in close proximity to the implants. These sites serve as reservoirs for immune cell migration, in the event of inflammatory response. We observe no significant changes in the percentages of CD4+ T cells, B cells, CD8+ T cells and NK cells in the DLNs, for any examined case

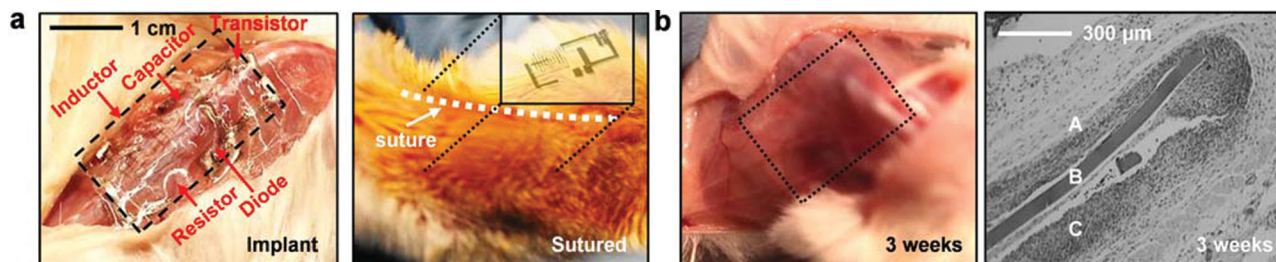


**Figure 4.** *In vivo* evaluation of a piece of transient electronics. (a) Images showing implanted (left) and sutured (right) transient circuit implanted in the sub-dermal region of a BALB-c mouse. (b) Implant site, 3 weeks after implantation (left). Histological section of tissue at the implant site, examined after 3 weeks showing integration of the silk film into subdermal layers (right). (A, subcutaneous tissue; B, silk film; C, muscle layer) Reproduced with permission.<sup>[9]</sup> 2013, Wiley.

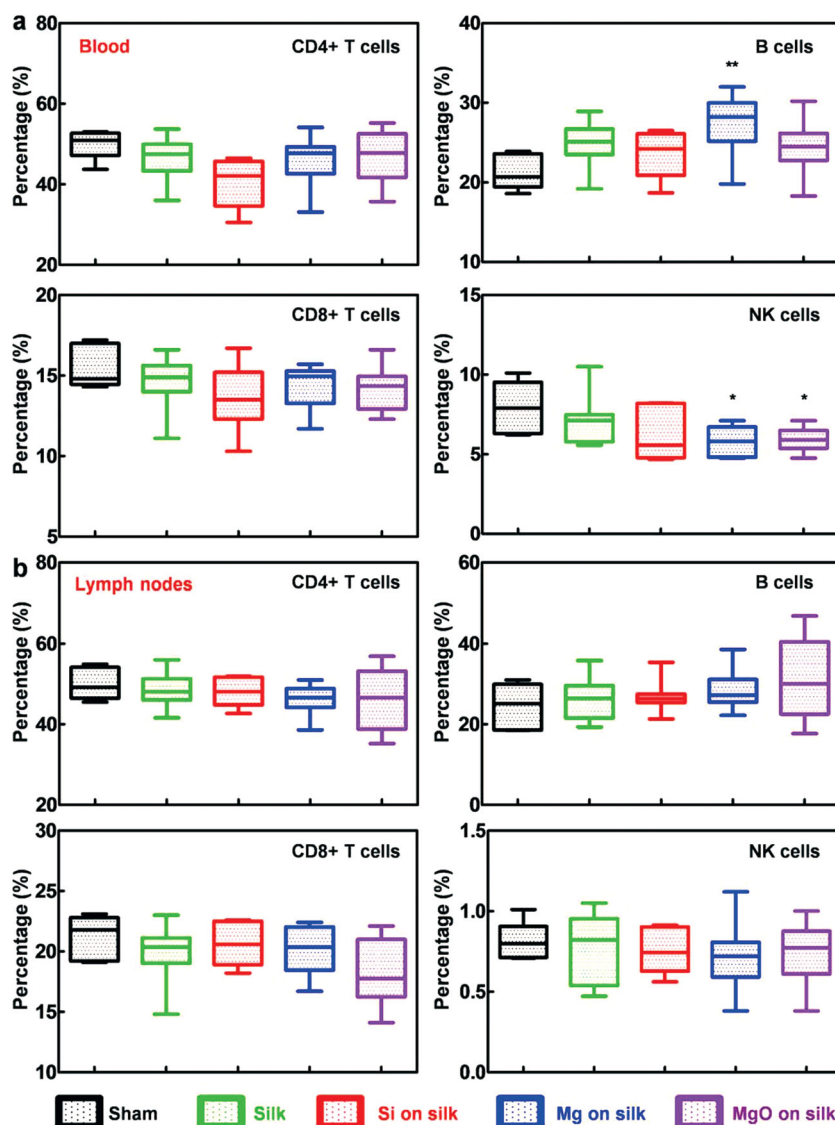


**Figure 5.** Systematic animal model studies of test structures built with transient electronic materials. Percentages of CD4+ T cells, B cells, CD8+ T cells and NK cells in the peripheral blood (a) and lymph nodes (b) of sham-operated mice and those with implanted transient test structures (silk, Si on silk, Mg on silk and MgO on silk) five weeks after implantation (\*,  $P < 0.05$ ).

(Figure 5b). Furthermore, serum levels of pro-inflammatory cytokines (IL-6, MCP-1, IFN- $\gamma$ , TNF- $\alpha$ , and IL-12p70) at 5 weeks post-implantation show no significant differences between implanted and sham-operated mice (Figure 6). Taken together, the data suggest that all four types of transient electronic test structures are biocompatible and non-immunogenic.

### 3. Conclusion

The materials presented here establish a baseline of capabilities for diverse types of electronic components, sensors, and options in power supply, all of which are completely soluble in water and biofluids. Studies of silicon dissolution suggest that the associated chemical processes depend on a number of chemical and physical factors, ranging from pH to ionic content to temperature and doping level in the silicon. Initial results from *in vivo* testing indicate the potential for use in active, biodegradable implants. Although many of the essential ideas are now available for this class of technology, there remain many opportunities for studying further the associated chemistry of transience, expanding the options in active and passive materials, creating devices designs that meet practical engineering requirements in both performance and mode of transience and inventing schemes for scalable manufacturing.

### 4. Experimental Section

*Studies of dissolution of single crystalline silicon nanomembranes (Si NMs):* A series of experiments were conducted to examine the dissolution kinetics of Si NMs in biofluids, and in aqueous solutions with different pH values and temperatures. Fabrication of the structures began with silicon-on-insulator (SOI, SOITEC, France) wafers with a

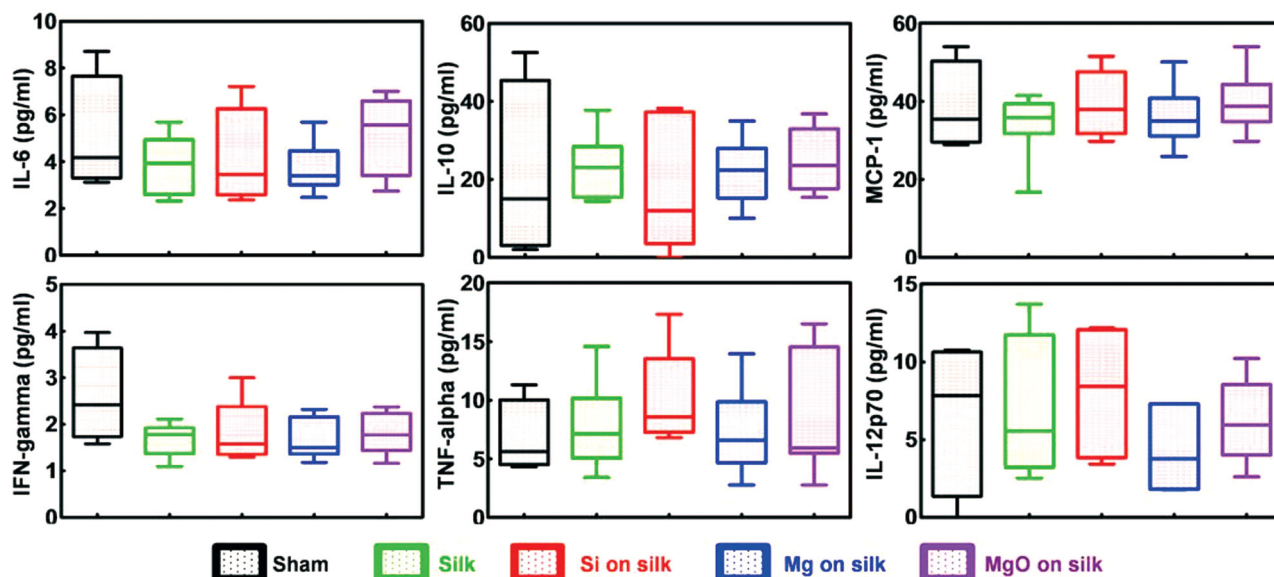


**Figure 6.** Systematic animal model studies of test structures built with transient electronic materials. Concentrations of pro-inflammatory cytokines, including IL-6, IL-10, MCP-1, IFN- $\gamma$ , TNF- $\alpha$ , and IL-12p70, detected from peripheral blood after 5 weeks of subcutaneous implantation of four types of transient electronic materials (silk, Si on silk, Mg on silk and MgO on silk).

~320 nm thick top silicon layer (p-type 10–20  $\Omega$ -cm). Repetitive dry oxidation at 1100  $^{\circ}$ C and wet etching in hydrofluoric acid (HF) thinned the top silicon to ~70 nm. Next, photolithography and reactive ion etching with sulfur hexafluoride patterned the top silicon into an array of squares ( $3 \mu\text{m} \times 3 \mu\text{m} \times 70 \text{nm}$ ) on the  $\text{SiO}_2/\text{Si}$  substrate ( $1 \text{cm} \times 1.5 \text{cm}$ ). The samples were placed into 50 mL of buffer solutions (PBS, pH 6 to 14, Sigma-Aldrich, USA) or a biofluid (bovine serum, Sigma-Aldrich, USA) at either room temperature or body temperature (37  $^{\circ}$ C). The samples were removed from the solutions, rinsed thoroughly with DI water, and then measured by atomic force microscopy (AFM, Asylum Research MFP-3D, USA) to determine the thickness and the surface roughness. After AFM measurements, the samples were returned to the aqueous solutions. The solution was replaced every other day.

**Aqueous buffer solutions:** Aqueous buffer solutions with different pH values were purchased to conduct dissolution tests of Si NMs. pH 6.0 (20  $^{\circ}$ C) - citric acid/sodium hydroxide solution (Sigma-Aldrich, USA), pH 7.0 (20  $^{\circ}$ C) - potassium dihydrogen phosphate/disodium hydrogen phosphate (Sigma-Aldrich, USA), pH 8.0 (20  $^{\circ}$ C) - borax/hydrochloric acid (Sigma-Aldrich, USA), pH 10.0 (20  $^{\circ}$ C) - di-sodium tetraborate/sodium hydroxide (Sigma-Aldrich, USA), pH 12.0 (20  $^{\circ}$ C) - di-sodium hydrogen phosphate/sodium hydroxide solution (Sigma-Aldrich, USA), pH 13.0 (20  $^{\circ}$ C) - glycine/sodium hydroxide/sodium chloride solution (Sigma-Aldrich, USA), pH 14.0 (20  $^{\circ}$ C) - sodium hydroxide was added to pH 13.0 to adjust the pH value. Phosphate buffer solution - 1.0 M, pH 7.4 (25  $^{\circ}$ C); pH 7.3 - 7.5; molar concentration of phosphate (0.95 - 1.05 M) (Sigma-Aldrich, USA), Phosphate buffer solution - 0.1 M; pH 7.45 - 7.55 (Sigma-Aldrich, USA), Phosphate buffer solution - 0.05 M; pH 7.5, containing  $\text{K}_2\text{HPO}_4$  and  $\text{KH}_2\text{PO}_4$  (Sigma-Aldrich, USA). We note that the property of phosphate buffer solution (1M, pH 7.4) was recently changed/modified, thereby leading to a change in the dissolution rate. The detailed chemistry of these solutions is not readily available from Sigma-Aldrich.

**Fabrication of the samples for implantation:** Four different types of samples (silk, Si on silk, Mg on silk, MgO on silk) were used for in vivo testing. Si NMs (~70 nm) with various shapes were fabricated from SOI wafers using the procedures outlined in the previous section. To release the patterned Si NMs, the buried oxide was partially etched with hydrofluoric acid (HF, 49% Electronic grade, ScienceLab, USA). A layer of photoresist (AZ 5214) formed anchor bars ( $10 \mu\text{m} \times 500 \mu\text{m}$ , 1.5  $\mu\text{m}$  thick) that tethered the Si NMs to the underlying substrate while completing the

removal of the buried oxide by immersion in HF. The resulting Si NMs were transfer printed onto a film of silk on a silicon wafer (as a temporary 'carrier' substrate). Thin layers of Mg (~300 nm) and MgO (~300 nm) with diverse shapes were deposited by electron-beam evaporation onto silk substrates through high resolution shadow masks made from polyimide (PI) films (12.5  $\mu\text{m}$ , Kapton, Dupont, USA). In all cases, the patterned geometries included squares, triangles, stars and circles.

**Surgical procedures:** All animal experiments were approved by Institutional Animal Care and Use Committees of Korea University (KUIACUC-2013-93) and performed in accordance with national and institutional guidelines. The animals were anesthetized with a mixture of 30 mg/kg zolazepam hydroxide (Zoletil 50; Virbac, Sao Paulo, Brazil) and 10 mg/kg xylazine hydroxide (Rumpun; Bayer, Shawnee Mission, KS) via intraperitoneal injection. After the induction of anesthesia, the hair on the back was shaved around the implantation site and the skin was sterilized by brushing with a 70% ethanol solution. Incisions were made with scissors, for subcutaneous insertion of HPDE films and transient electronic test structures. Control animals were treated by a sham operation with no implantation.

**Flow cytometry analyses:** CD4+CD3+ T cells, CD8+CD3+ T cells, CD19+CD3- B cells and Dx5+CD3- NK cells were detected by staining in 100  $\mu\text{L}$  of FACS buffer (PBS containing 2% FBS and 0.02% sodium azide) with antibodies against anti-mouse CD4 (RM4-4)-PE, CD8 (53-6.7)-APC-Cy7, CD3 (145-2C11)-APC, CD19 (1D3)-PerCP and CD49b (Dx5)-PE-Cy7 (eBioscience, CA, USA). Flow cytometry was carried out with a FACSCantoII (BD Biosciences, San Diego, CA, USA) and the data were analyzed with Flowjo software (Three Star, USA).

**Cytometric Bead Arrays (CBA) for measuring cytokine s:** Serum concentrations of IL-6, IL-10, MCP-1, IFN- $\gamma$ , TNF and IL-12p70 were measured using a CBA Mouse Inflammation Kit (BD Biosciences, San Diego, CA), according to the manufacturer's instructions. Before sacrificing the animals at 5 weeks, peripheral blood was collected in vacutainers by retro-orbital bleeding and serum was separated by centrifugation at 5000 rpm for 10 minutes.

**Statistics:** All data are reported as mean  $\pm$  standard error (SEM). Analysis used Prism software (Graph Pad Prism 5.0). Statistical significance was determined by one-way analysis of variance (ANOVA) followed by Dunnett's multiple comparison test. When P value was less than 0.05, the result was considered significant (\*,  $P < 0.05$ ).

## Acknowledgements

This article is part of a series celebrating the 25<sup>th</sup> anniversary of *Advanced Materials*. S.-W. Hwang and G. Park contributed equally to this work. Huanyu Cheng is a Howard Hughes Medical Institute International Student Research fellow. The new work was supported by an NSF INSPIRE grant, a grant from DARPA and the Korea Foundation for International Cooperation of Science & Technology (KICOS) grant (K20703001994-12A0500-03610), NRF-2013M3A9D3045719 and the Converging Research Center Program (2013K000268). The facilities for characterization and analysis were provided by the Material Research Laboratory and Center for Microanalysis of Materials at the University of Illinois at Urbana-Champaign, both of which are supported by the U.S. Department of Energy.

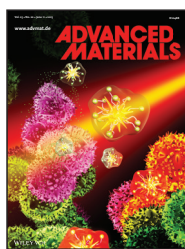
Received: September 26, 2013

Revised: November 13, 2013

Published online: February 21, 2014

- 
- [1] D.-H. Kim, Y.-S. Kim, J. Amsden, B. Panilaitis, D. L. Kaplan, F. G. Omenetto, M. R. Zakin, J. A. Rogers, *Appl. Phys. Lett.* **2009**, *95*, 133701.
- [2] D.-H. Kim, J. Vimenti, J. Amsden, J. Xiao, L. Vigeland, Y.-S. Kim, J. A. Blanco, B. Panilaitis, E. S. Frechette, D. Contreras, D. L. Kaplan, F. G. Omenetto, Y. Huang, K.-C. Hwang, M. R. Zakin, B. Litt, J. A. Rogers, *Nat. Mater.* **2010**, *9*, 511.
- [3] C. J. Bettinger, Z. Bao, *Adv. Mater.* **2010**, *22*, 651.
- [4] M. Irimia-Vladu, P. A. Troshin, M. Reisinger, L. Shmygleva, Y. Kanbur, G. Schwabegger, M. Bodea, R. Schwödäuer, A. Mumyatov, J. W. Fergus, V. F. Razumov, H. Sitter, N. S. Sariciftci, S. Bauer, *Adv. Funct. Mater.* **2010**, *20*, 4069.
- [5] E. J. Anglin, L. Cheng, W. R. Freeman, M. J. Sailor, *Adv. Drug Deliver. Rev.* **2008**, *60*, 1266.
- [6] J.-H. Park, L. Gu, G. V. Maltzahn, E. Ruoslahti, S. N. Bhatia, M. J. Sailor, *Nat. Mater.* **2009**, *8*, 331.
- [7] S.-W. Hwang, H. Tao, D.-H. Kim, H. Cheng, J.-K. Song, E. Rill, M. A. Brenckle, B. Panilaitis, S. M. Won, Y.-S. Kim, Y. M. Song, K. J. Yu, A. Ameen, R. Li, Y. Su, M. Yang, D. L. Kaplan, M. R. Zakin, M. J. Slepian, Y. Huang, F. G. Omenetto, J. A. Rogers, *Science* **2012**, *337*, 1640.
- [8] S.-W. Hwang, X. Huang, J.-H. Seo, J.-K. Song, S. Kim, S. Hage-Ali, H.-J. Chung, H. Tao, F. G. Omenetto, Z. Ma, J. A. Rogers, *Adv. Mater.* **2013**, *25*, 3526.
- [9] S.-W. Hwang, D.-H. Kim, H. Tao, T.-I. Kim, S. Kim, K. J. Yu, B. Panilaitis, J.-W. Jeong, J.-K. Song, F. G. Omenetto, J. A. Rogers, *Adv. Funct. Mater.* **2013**, *23*, 4087.
- [10] C. Dagdeviren, S.-W. Hwang, Y. Su, S. Kim, H. Cheng, O. Gur, R. Haney, F. G. Omenetto, Y. Huang, J. A. Rogers, *Small* **2013**, *9*, 3398.
- [11] L. Yin, H. Cheng, S. Mao, R. Haasch, Y. Liu, X. Xie, S.-W. Hwang, H. Jain, S.-K. Kang, Y. Su, R. Li, Y. Huang, J. A. Rogers, *Adv. Funct. Mater.* DOI: 10.1002/adfm.201301847.
- [12] H. Seidel, L. Csepregi, A. Heuberger, H. Baumgartel, *J. Electrochem. Soc.* **1990**, *137*, 3612.
- [13] J. D. Rimstidt, H. L. Barnes, *Geochim. Cosmochim. Ac.* **1980**, *44*, 1683.
- [14] K. S. Finnie, d. j. Waller, F. L. Perret, A. M. Krause-Heuer, H. Q. Lin, J. V. Hanna, C. J. Barbe, *J. Sol-Gel Sci. Technol.* **2009**, *49*, 12.
- [15] M. Morita, T. Ohmi, E. Hasegawa, M. Kawakami, M. Ohwada, *J. Appl. Phys.* **1990**, *68*, 1272.
- [16] N. F. Raley, Y. Sugiyama, T. Van Duzer, *J. Electrochem. Soc.* **1984**, *131*, 161.
- [17] E. D. Palik, V. M. Bermudez, O. J. Glembocki, *J. Electrochem. Soc.* **1985**, *132*, 135.
- [18] E. D. Palik, V. M. Bermudez, O. J. Glembocki, *J. Electrochem. Soc.* **1985**, *132*, 871.
- [19] H. Seidel, L. Csepregi, A. Heuberger, H. Baumgartel, *J. Electrochem. Soc.* **1990**, *137*, 3626.
- [20] E. Vazsonyi, Z. Vertesy, A. Toth, J. Szlufcik, *J. Micromech. Microeng.* **2003**, *13*, 165.
- [21] S. H. C. Anderson, H. Elliott, D. J. Wallis, L. T. Canham, J. J. Powell, *Phys. status solidi A* **2003**, *197*, 331.
- [22] K. R. Williams, K. Gupta, M. Wasilik, *J. Microelectromech. S.* **2003**, *12*, 761.
- [23] P. M. Dove, D. A. Crerar, *Geochim. Cosmochim. Ac.* **1990**, *54*, 955.
- [24] B. A. Fleming, *J. Colloid. Interf. Sci.* **1986**, *110*, 40.
-

## Top Journals and their 2012 Impact Factors\*

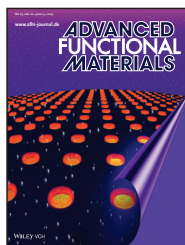


App to be launched soon!

### Advanced Materials

**Impact Factor: 14.829**

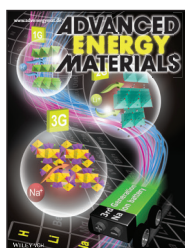
One key to the success of *Advanced Materials* is its pronounced interdisciplinary, manifested in its rare listing in six different subject categories. It is ranked #1 with 91,952 citations in Nanoscience & Nanotechnology and ranked #2 in Multidisciplinary Materials Science.



### Advanced Functional Materials

**Impact Factor: 9.765**

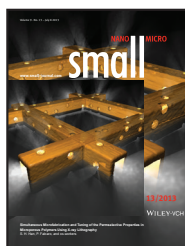
*Advanced Functional Materials* reinforces its standing as a leading full-paper general materials science journal.



### Advanced Energy Materials

**First Impact Factor: 10.043**

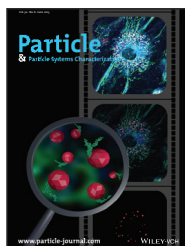
*Advanced Energy Materials* received its first Impact Factor of 10.043. It confirms in numbers that *Advanced Energy Materials* has joined *Advanced Materials*, *Advanced Functional Materials* and *Small* as top quality journal, publishing in the field of energy-related research.



### Small

**Impact Factor: 7.823**

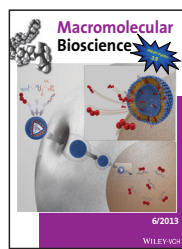
With an Impact Factor of 7.823, *Small* continues to be the premier journal for research at the nano- and microscale.



### Particle

**Impact Factor: 0.857**

*Particle*, a member of the *Advanced* journals family, focuses on all aspects of particle research. It is one of the top 10 journals in Characterization & Testing by Impact Factor and by total citations, too.



### Macromolecular Bioscience

**Impact Factor: 3.742**

*Macromolecular Bioscience* is ranked among the top 5 biomaterials journals and listed among the top 10 polymer journals. It maintains its position as the leading journal at the intersection of materials and polymer science with life sciences and medicine.



### Journal of Biomedical Materials Research, Part A

**Impact Factor: 2.834**

It is ranked #2 with 12,128 citations in Biomaterials. Published on behalf of the *Society for Biomaterials*.

### Journal of Biomedical Materials Research, Part B

**Impact Factor: 2.308**

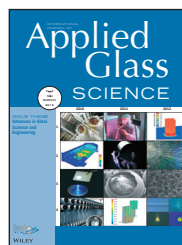
Published on behalf of the *Society for Biomaterials*.



### Journal of the American Ceramic Society

**Impact Factor: 2.107**

The journal continues to far outpace all other Ceramic related journals with over 30,500 total cites! Published on behalf of the *The American Ceramic Society*.

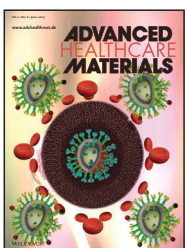


### International Journal of Applied Glass Science

**First Impact Factor: 1.548**

The journal received its first Impact Factor of 1.548 and has established itself as an indispensable source of knowledge on the application of glass science and engineering across the entire materials spectrum. Published on behalf of *The American Ceramic Society*.

## NEW JOURNALS



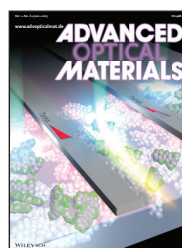
### Advanced Healthcare Materials

**First Immediacy Index: 0.712**

Launched in 2012, *Advanced Healthcare Materials* received its first Immediacy Index of 0.712. This inaugural value establishes *Advanced Healthcare Materials* as a premier journal for publishing biomedical materials research.

[www.advhealthmat.com](http://www.advhealthmat.com)

Get complimentary online access in 2013:  
[wileyonlinelibrary.com/newjournals-optin](http://wileyonlinelibrary.com/newjournals-optin)



### Advanced Optical Materials

**First Immediacy Index will be announced in 2014.**

This new journal was founded in 2013 as a member of the *Advanced* journals family. It is covering all aspects of light-matter interactions, including topics like plasmonics, metamaterials, photonics and more.

[www.advopticalmat.com](http://www.advopticalmat.com)

Get complimentary online access in 2013&2014:  
[wileyonlinelibrary.com/newjournals-optin](http://wileyonlinelibrary.com/newjournals-optin)

[wileyonlinelibrary.com/subject/materials](http://wileyonlinelibrary.com/subject/materials)